Structural features of the Middle Tirso Valley (Central Sardinia - Italy) from geoelectrical and gravity data

Teresa Andriani ([1]), **Roberto Balia** ([2]), **Mariano Loddo** ([1]), **Giuseppe Pecorini** ([3]) **and Antonio Tramacere** ([1])

([1]) *Dipartimento di Geologia e Geofisica, Università di Bari, Italy*

([2]) *Dipartimento di Ingegneria del Territorio, Università di Cagliari, Italy*

([3]) *Dipartimento di Scienze della Terra, Università di Cagliari, Italy*

Abstract

The Middle Tirso Valley is located in Central Sardinia and lies between two structural highs, the Marghine-Goceano chain and the Barbagia Paleozoic horst. The geological structures of the area, potentially interesting for its geothermal resources, are rather complex and dominated by two regional faults – the Marghine fault and the Nuoro fault – which affect the Palaeozoic basement and the Tertiary volcano-sedimentary deposits. Combined modelling of gravity and geoelectrical data defines the shape and extent of this Tertiary basin. The Bouguer anomaly is mainly characterized by a three-dimensional gravity low which has been named «Bolotana-Sedilo gravity low», corresponding to a structure generated by collapses attributable to transcurrent and extensional tectonic events. The down faulted zone is filled with a Tertiary low density volcano-sedimentary sequence extending southwards and overlain by Pliocene-Quaternary basalts. Another regional structure named «Tirso Fault» is proposed

Key words *gravity survey – geoelectrical soundings – Sardinia*

1. Introduction and geological setting

The Middle-Tirso Valley (fig. 1) is located in Central Sardinia. It is a tectonic depression (Cherchi and Montadert, 1982; Pala *et al.*, 1982) mainly filled with calk-alkaline volcanic products (Upper Oligocene - Lower Middle Miocene) and continental deposits (Lower Miocene). The Plio-Quaternary cover consists of basaltic lava flows and terraced alluvial deposits. From a structural point of view the Middle Tirso Valley is bounded by the Marghine and the Nuoro faults. It extends NE-SW between the Paleozoic horsts of the Marghine-Goceano chain and the Barbagia in a direction perpendicular to the main N-S trending regional structures of Sardinia (Oggiano *et al.*, 1995).

The geological and structural complexity of the area is the result of several events (Coulon *et al.*, 1978; Beccaluva *et al.*, 1987) among which: 1) the Oligo-Miocene calkalkaline magmatism; 2) NE-SW trending sinistral transcurrent tectonics, which affected the area in the Oligocene-Lower Miocene; 3) extensional tectonics dating to the Early-Middle Miocene related to the rotation of the Corse-Sardinian block during the Burdigalian, which led to the formation of the Sardinian Rift; 4) the Upper Miocene-Pleistocene extension with the formation of the Campidano Graben and Pliocene-Pleistocene volcanism.

Mailing address: Prof. Antonio Tramacere, Dipartimento di Geologia e Geofisica, Università di Bari, Campus Universitario, Via E. Orabona 4, 70125 Bari, Italy; e-mail: a.tramacere@geo.uniba.it

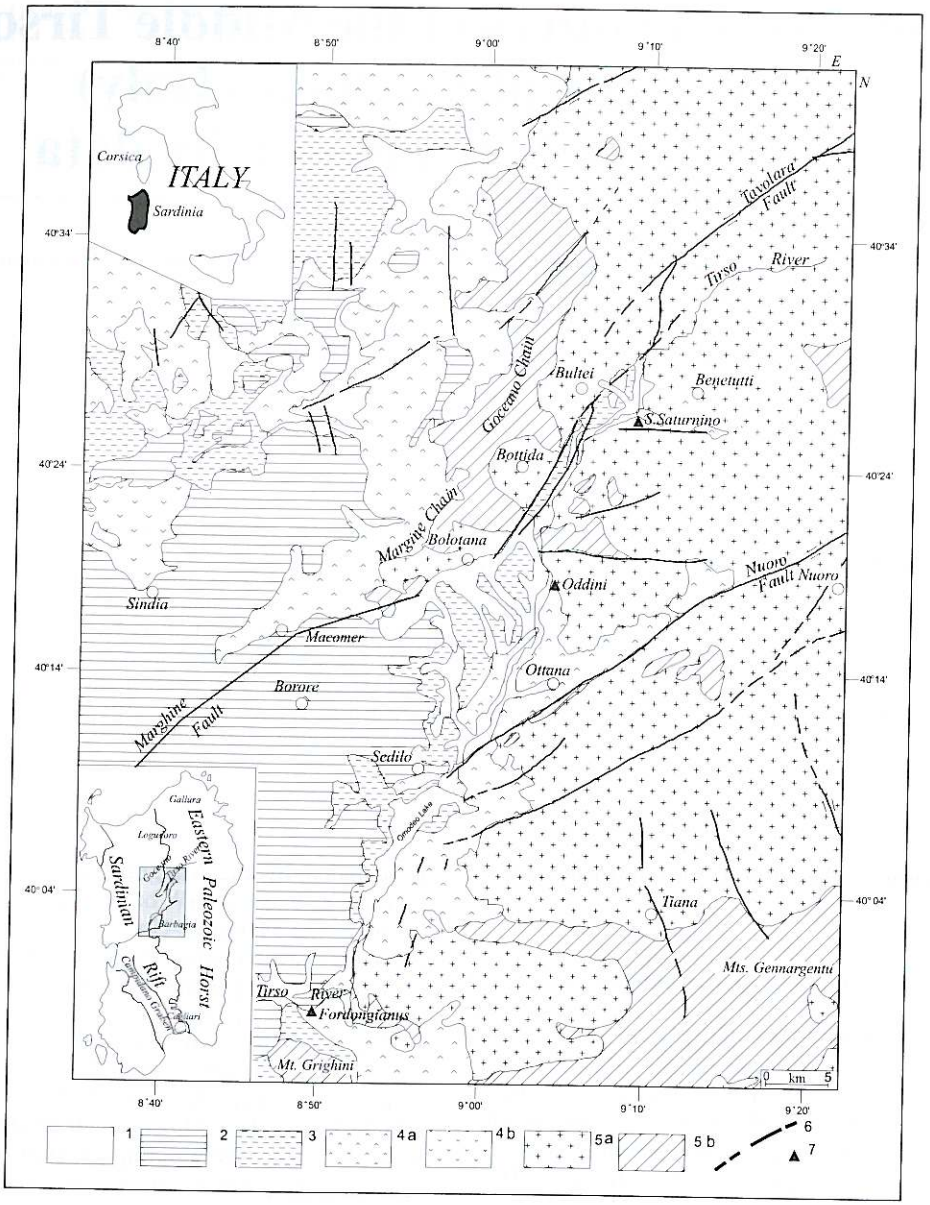

Fig. 1. Schematic geological map of the Middle-Tirso Valley (after Carmignani, 1996, modified): 1) Quaternary sediments (Holocene), alluvial cones and terraced fluvial sediments (Pliocene-Pleistocene). 2) Pliocene-Pleistocene alkaline and transitional basalts and undersaturated volcanic rocks. 3) Miocene continental and marine deposits (Burdigalian-Middle to Upper Langhian) and continental deposits with rhyolitic tuff intercalations (Aquitanian-Burdigalian). 4) Oligo-Miocene calcalkaline volcanic cycles: 4a) Ignimbrites, tuffites and pumiceous tuffites (Upper Oligocene-Lower to Middle Miocene); 4b) Andesites (Upper Oligocene-Lower Miocene). 5) Hercynian basement: 5a) Paleozoic granitoids (Upper Carboniferous-Permian); 5b) Paleozoic schists (Lower Carboniferous-Pre- to Upper Ordovician). 6) Faults. 7) Geothermal springs.

The relation between the Apennine collision, the transcurrent, both extensional and compressional structures in Northern-Central Sardinia (Pasci, 1997), the rifting and the drift of the Corse-Sardinian block, are still not fully understood.

The Paleozoic basement consists of the Hercynian metamorphic and intrusive complexes. The metamorphic rocks crop out mainly in the *Goceano chain* and in the *Grighini* and *Gennargentu mountains*. They are composed of Ordovician acidic to calkalcaline metavolcanic rocks and Cambrian-Lower Carboniferous metasedimentary and sedimentary rocks containing Silurian-Devonian alkaline metabasites (Oggiano, 1994). The granitoid bodies of the plutonic complex (Upper Carboniferous-Permian) vary from quarzodioritic tonalite to granodiorite and granite (Ghezzo *et al.*, 1973).

The Oligocene-Miocene volcanic rocks, mainly ignimbrites and andesites, lie directly on the Paleozoic basement, with no trace of Mesozoic rocks (Porcu, 1983).

The ignimbrites are overlain by a continental sequence made up of cherty limestones, siltstones, sandstones and fluvial conglomerates alternating with cherts, tuffites and pumiceous tuffites (Aquitanian - Burdigalian). A continental to marine sequence follows, consisting of marls, sandstones, conglomerates and sublittoral-epibathyal siliceous sandstones dating to the Upper Burdigalian - Middle Upper Langhian (Carmignani, 1996).

The Pliocene-Pleistocene volcanic rocks, cropping out in the western side of the area, are represented by alkaline to transitional basalts with fluvial-lacustrine sediments on the bottom and between the lava flows (Carmignani, 1996).

Quaternary rocks occur as alluvial and colluvial deposits; Pliocene-Pleistocene fluvial terraces are also commonly found along the Tirso River course.

Therefore, the study of the Middle Tirso Valley was considered interesting to contribute to the general knowledge of geological and structural features of Sardinia and the geodynamic evolution of the Western Mediterranean basin.

From a more practical point of view, the area is interesting for its hydrogeology and geothermal potential, the latter witnessed by the San Saturnino, Oddini and Fordongianus geothermal springs (fig. 1), whose origin is still not fully defined.

Combined geoelectrical and gravity modelling of the area has been performed to gain information on the above aspects.

2. Acquisition of geoelectrical data

The subsurface resistivity distribution was obtained by means of twenty-five axial dipole-dipole electrical soundings (DES, *e.g.*, see Alpin, 1966), with dipole-dipole separation in the range 100-10000 m. They were located so as to obtain a main section, striking roughly NE-SW (profile R-CT), and three transverse sections striking roughly NW-SE (profiles T-T′, A-A′ and B-B′) across the Tirso River (fig. 2).

A 3.2 kVA D.C. generator with output voltage steps ranging from 50 to 1000 V was used. The main features of the data acquisition system were a notch filter, a band-pass filter and an A/D converter with precision of 0.1 μV.

In order to achieve an effective signal from noise separation, repeated square waveforms with 30 s period were used, with simultaneous recording at the receiving dipole. The record length was 15-60 min, depending on noise level, with a sampling interval of 0.1 s.

In order to obtain reliable signal estimates to be used in the apparent resistivity computation, three different methods, namely the FFT, the Maximum Likelihood Method (Loddo and Patella, 1977) and the MEM spectral analysis (Lacoss, 1971) were used.

2.1. *Analysis of geoelectrical data*

The relative error affecting the resistivity estimates was in the order of 4-10%, depending on noise level. The complete set of apparent resistivity curves (ρ_a *versus* dipole-dipole spacing in the range 100-10000 m) is shown in fig. 3a-d. The low wavenumber scattering of apparent resistivity values is attributable to vertical contacts between rocks with different resistivity, crossed by the receiving dipole path.

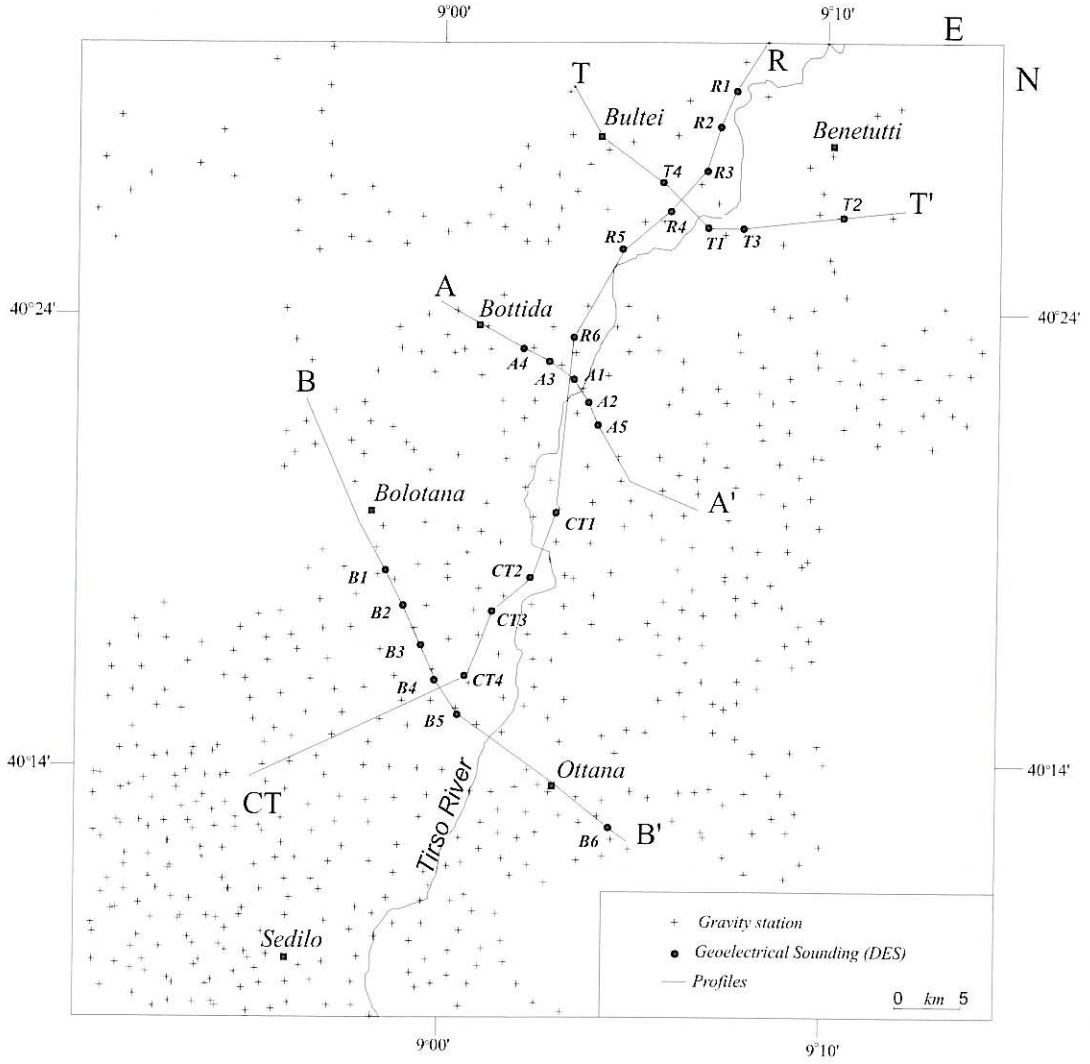

Fig. 2. Location of gravity stations and dipole-dipole geoelectrical soundings along profiles T-T′, A-A′, B-B′ and R-CT.

The apparent resistivity pseudosections are reported in fig. 4a-d. These pseudosections were obtained, for each profile, assigning the logarithm of the measured apparent resistivity to points having as horizontal and vertical coordinates the position of the receiving dipole (fixed for each sounding) and the dipole-dipole separation, respectively, and finally applying a contouring procedure.

Pseudosections relating to profiles T-T′ and A-A′, which are almost perpendicular to the Tirso River, show lower values on the western side, that is W of its course, and higher values on the opposite side. This indicates that in this area the

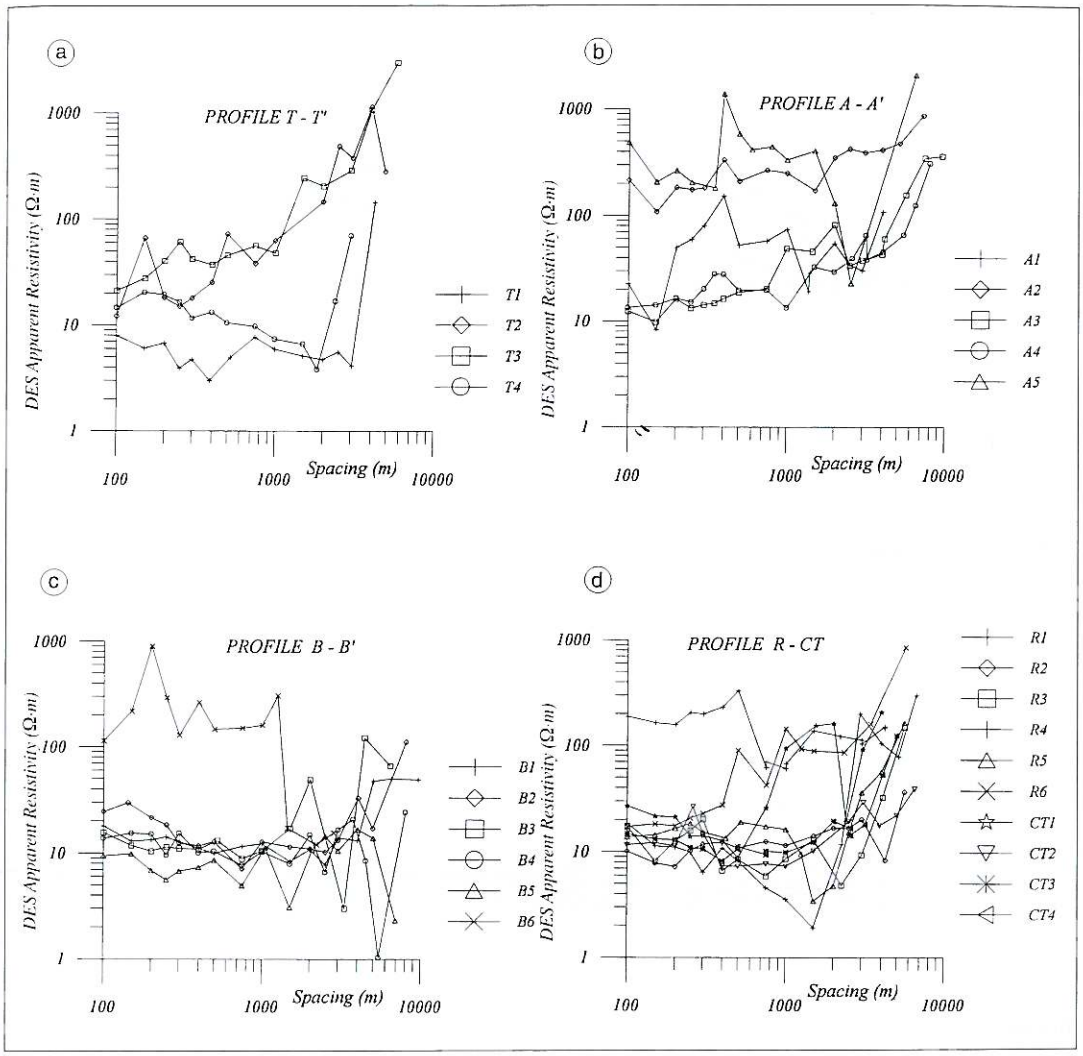

Fig. 3a-d. Axial dipole apparent resistivity diagrams: a) profile T′-T′; b) profile A-A′; c) profile B-B′; d) profile R-CT.

river runs along a shallow contact between rocks with different electrical characteristics, namely resistive granitoid rocks on the east bank and less resistive volcano-sedimentary and metamorphic rocks on the west bank. Similar findings were obtained for the pseudosection B-B′ where the river runs between soundings B5 and B6 and a wide low resistivity area is present on the west side.

The pseudosection relating to profile R-CT, which is almost parallel to the river, shows a rather different structure with two relative minimum resistivity basins, the southernmost of which is particularly evident, separated by a broad resistive structure.

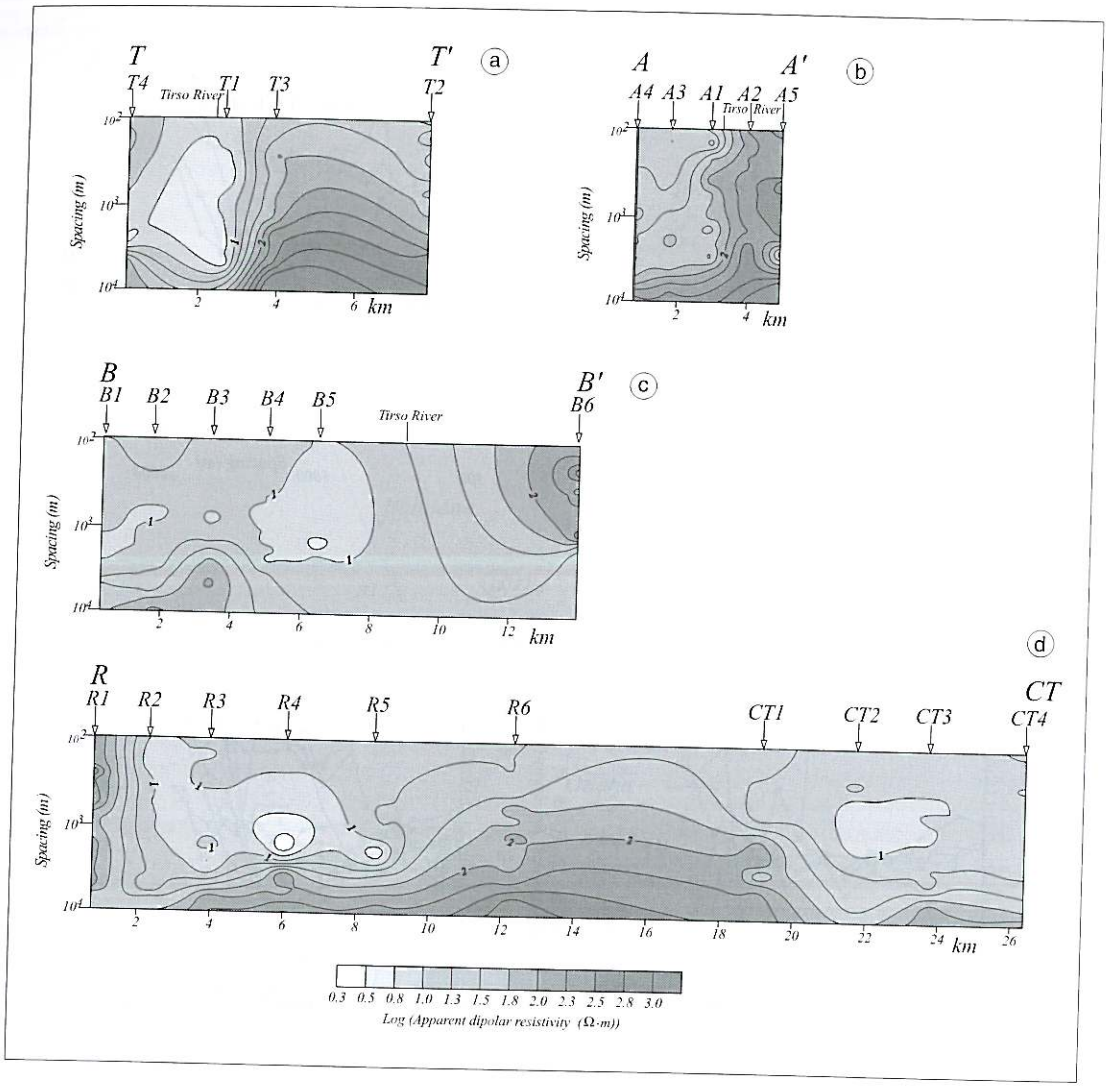

Fig. 4a-d. Apparent resistivity pseudosections: a) profile T-T′; b) profile A-A′; c) profile B-B′; d) profile R-CT. Arrows indicate the position of the fixed receiving dipole corresponding to each sounding.

2.2. *Inversion and interpretation*

Quantitative 1D inversion of experimental data was generally performed by means of a ridge regression procedure (Meju, 1992), as shown in fig. 5a for sounding CT3. On the other hand, the Patella and Tramacere procedure (1986) was used for apparent resistivity curves characterized by steep slopes and/or strong apparent resistivity steps generated by vertical contacts, as for sounding R1 in fig. 5b. In this figure, the model adopted for fitting the experimental curve is also shown. It consists of two electrically different, layered structures

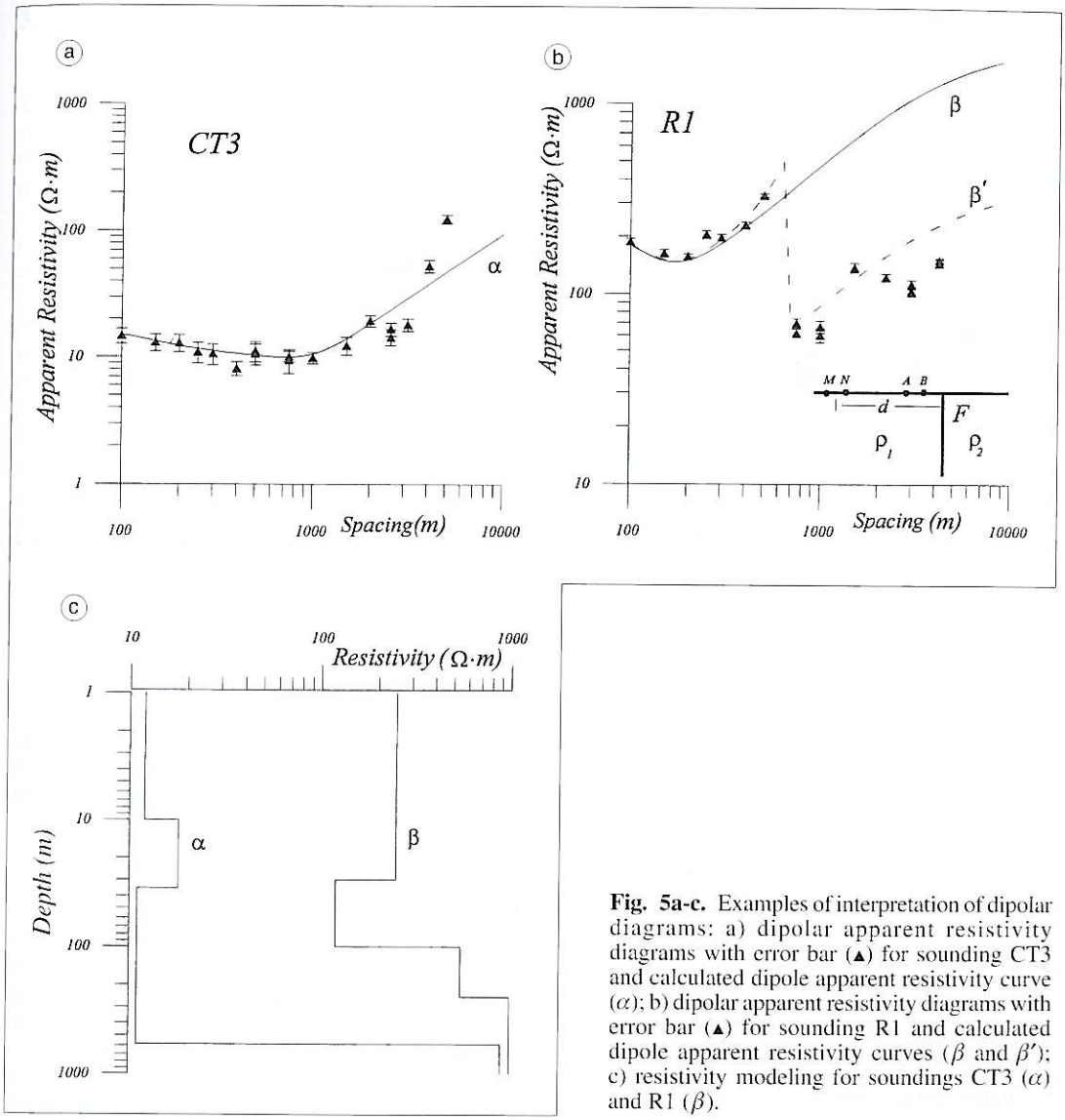

Fig. 5a-c. Examples of interpretation of dipolar diagrams: a) dipolar apparent resistivity diagrams with error bar (▲) for sounding CT3 and calculated dipole apparent resistivity curve (α); b) dipolar apparent resistivity diagrams with error bar (▲) for sounding R1 and calculated dipole apparent resistivity curves (β and β'); c) resistivity modeling for soundings CT3 (α) and R1 (β).

($\rho_2 = 0.1\ \rho_1\ \Omega\cdot$m), separated by a vertical contact about 700 m from the fixed potential dipole MN, which is crossed by the moving current dipole AB. This kind of model modifies the 1D theoretical curve β, from the resistivity step onward, into the β' curve, providing the best fit with experimental data. Figure 5c shows the 1D resistivity models obtained for the above soundings.

Resistivity cross-sections for all profiles are reported in fig. 6. On the basis of available geological and structural information and also referring to previous geophysical works concerning the surrounding areas of Logudoro

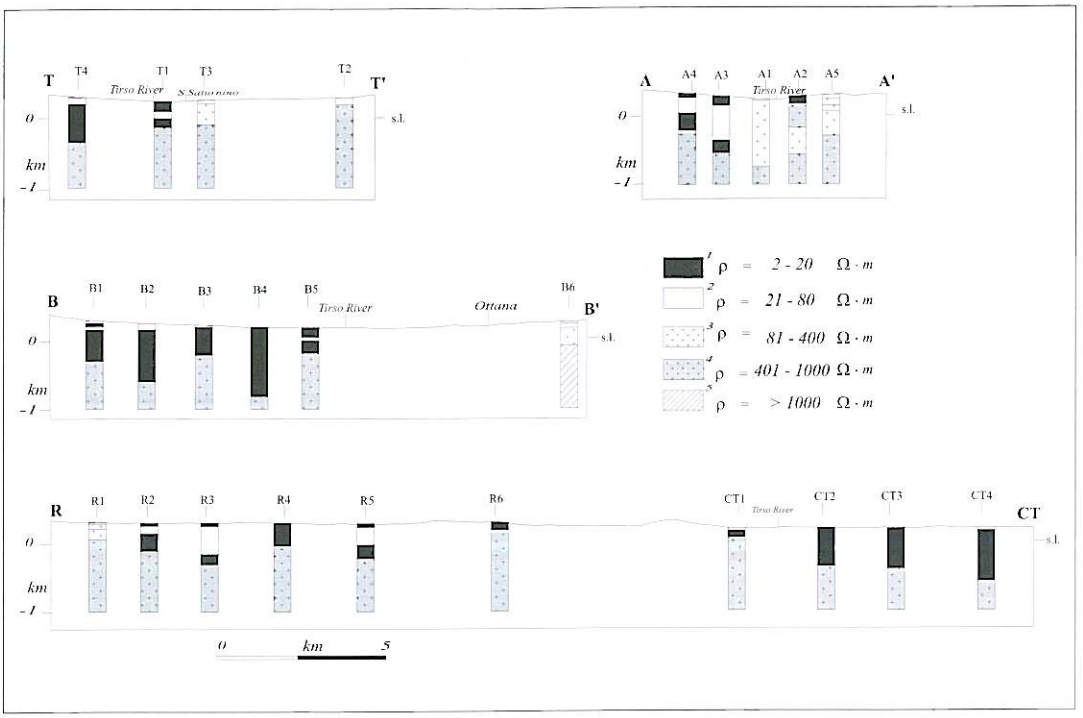

Fig. 6. Electrostratigraphic cross-sections for T-T′, A-A′, B-B′ and R-CT profiles. 1) Oligo-Miocene volcanic rocks and subordinate clastic sediments; 2) tuffaceous Oligo-Miocene volcanic rocks and pumiceous ash; 3), 4) more or less weathered and fractured Paleozoic granitoids and schistose metamorphic rocks; 5) massive Paleozoic granitoids.

(Pecorini *et al.*, 1988) and Fordongianus (Balia *et al.*, 1990), resistivity values and geological units were associated as follows:

1) 2 ÷ 20 (Ω·m)
   Oligo-Miocene volcanic rocks and subordinate clastic sediments.
2) 21 ÷ 80 (Ω·m)
   Tuffaceous Oligo-Miocene volcanic rocks and pumiceous ash.
3) 81 ÷ 400 (Ω·m)
4) 401 ÷ 1000 (Ω·m)
   More or less weathered and fractured Paleozoic granitoids and schistose metamorphic rocks.
5) > 1000 (Ω·m)
   Massive Paleozoic granitoids.

Some meaningful considerations can be drawn from the above correlation. First, the top of the Paleozoic basement extends down to as much as 800 m below sea level and its morphology produces several local basins, clearly evident in profiles B-B′ and R-CT. Second, the same basement is locally affected by major, sub-vertical displacements, particularly evident in profile A-A′.

The conductive formations (2-20 Ω·m and 21-80 Ω·m) corresponding to the Oligo-Miocene volcano-sedimentary complex overlaying the Paleozoic basement are especially thick in the Bultei-Benetutti (R1-R6) and Bolotana-Ottana (CT1-CT4 and B1-B5) areas, the latter basin known as the Ottana Graben (Porcu, 1983).

3. Gravity survey

The gravity survey concerned an area of about 1300 km^2 with 618 stations, so that the average station density was in the order of 0.5 per km^2 (fig. 2). A Lacoste and Romberg model G gravity meter, with scale factor of 1.06 mGal/div was used. Five points of the first gravity survey of Sardinia (Trudu, 1962) were selected as reference stations. These stations had already been included in the International Gravity Standardization Net, 1971 (Morelli *et al.*, 1974) and hence in the First Order Italian Gravity Network (Marson and Morelli, 1978). The mean error affecting gravity measurements was estimated to be in the order of ± 0.03 mGal. Elevations were determined by trigonometric levelling, with a mean estimated error in the order of 0.2 m, using an AGA mod.14 Geodimeter and a Wild Model 12 Theodolite.

3.1. *Bouguer anomalies*

Gravity corrections were applied adopting the mean crustal density of 2.67 g/cm^3. Terrain correction was computed considering the vertical effect of polyhedral bodies (Okabe, 1979). Mean elevations were computed by means of a digital terrain model (DTM) at a scale of 1:10000 over a regular grid spacing of 50 m within a 2 km radius from each gravity station, a DTM at 1:25000 scale over a regular grid spacing of 250 m at distances ranging from 2 to 30 km and a DTM at 1:100000 or 1:750000 scale over a grid spacing of 500 m at distances ranging from 30 to 167 km. The Bullard reduction for spherical cap (LaFher, 1991) was applied. The Bouguer anomalies were computed referring to the 1980 International Gravity Formula (Moritz, 1984).

Figure 7 shows the Bouguer anomaly map where two well separated low areas can be distinguished:

1) The first, located in the south-western part of the map, is bordered on the north-western side by a strong SW-NE oriented horizontal gradient belt corresponding with the Marghine Fault. Conversely, there are no well-defined gravity structures that could be associated with the Nuoro fault. This could mean that, in this area, the vertical displacements associated with the Nuoro fault are not as pronounced as in the Marghine fault.

2) The second gravity low, located in the north-eastern part of the map, east of the village of Benetutti, remains open eastwards and shows regularly decreasing values corresponding to the outcropping granite basement.

The gravity high which separates the above lows, attains maximum amplitude NE of the village of Bolotana, where Paleozoic metamorphic schists of the Goceano chain crop out.

The Bouguer anomaly was separated into regional and residual components by means of two-dimensional filtering. In order to gain wider data coverage for computations, data for the neighbouring areas of Logudoro (Pecorini *et al.*, 1988) and Fordongianus (Balia *et al.*, 1990) were also used. The optimum cut-off wavelength of 30 km was determined by means of the Maximum Entropy spectral analysis method applied to several N-S and E-W profiles.

The residual anomaly map superimposed on the geological and structural map of the area covered by gravity measurements is reported in fig. 8. The wide gravity low in the south-western part of the map, named «Bolotana-Sedilo gravity low», is bounded by rather strong horizontal gradients, especially in the north-western edge (the Marghine-Goceano chain), and exhibits a marked 3D character.

The San Saturnino and Oddini geothermal springs lie on opposite sides with respect to the gravity high and therefore, very likely, there is no spatial correlation between them. However, both places correspond to high values of horizontal gradient and outcrops of Oligo-Miocene volcanic rocks, a situation which is common for geothermal springs in Sardinia.

3.2. *Modelling and interpretation*

Residual gravity anomaly was modelled along four profiles corresponding to the geoelectrical profiles, using Marquardt's semi-automatic inversion method for 2.5D density distribution with varying length of strike, developed by Webring (1985). This is a powerful and flex-

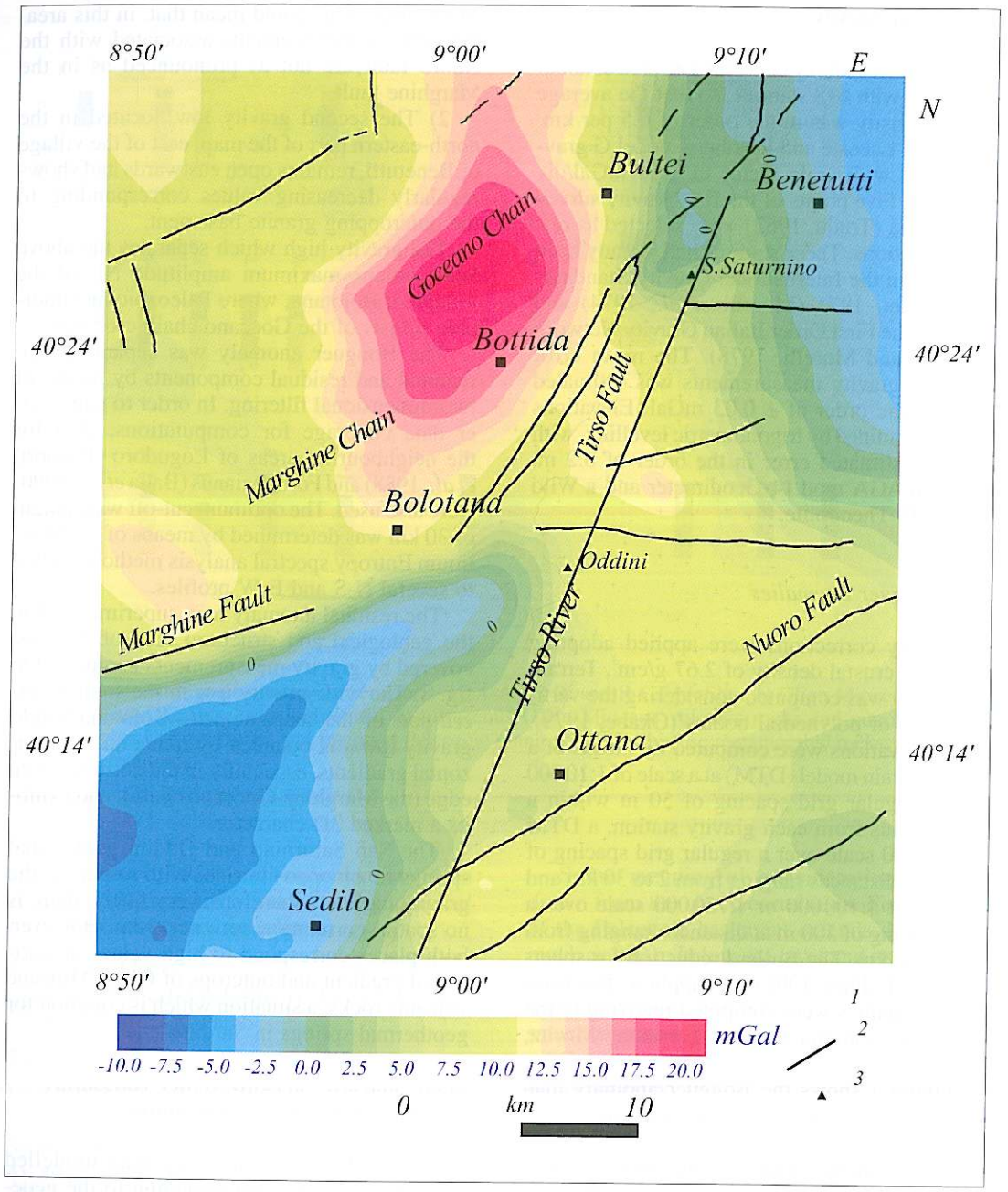

Fig. 7. Bouguer anomaly map of the Middle Tirso Valley. 1) gravity stations; 2) faults; 3) geothermal springs.

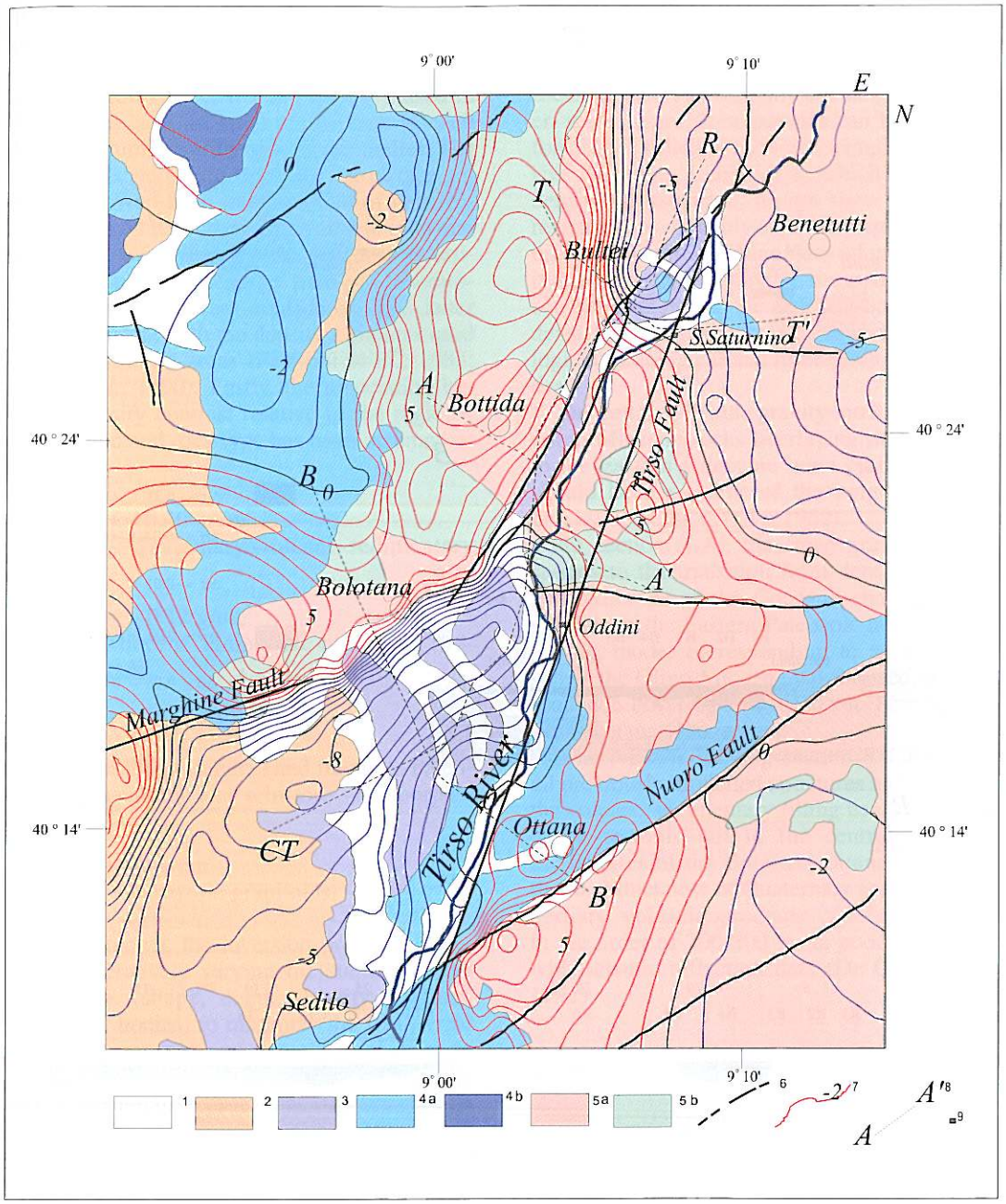

Fig. 8. Residual gravity anomaly map superimposed on the schematic geological map. For legend from 1 to 5b see fig. 1; 6) faults; 7) residual gravity anomaly contour lines; 8) gravity profiles; 9) geothermal springs.

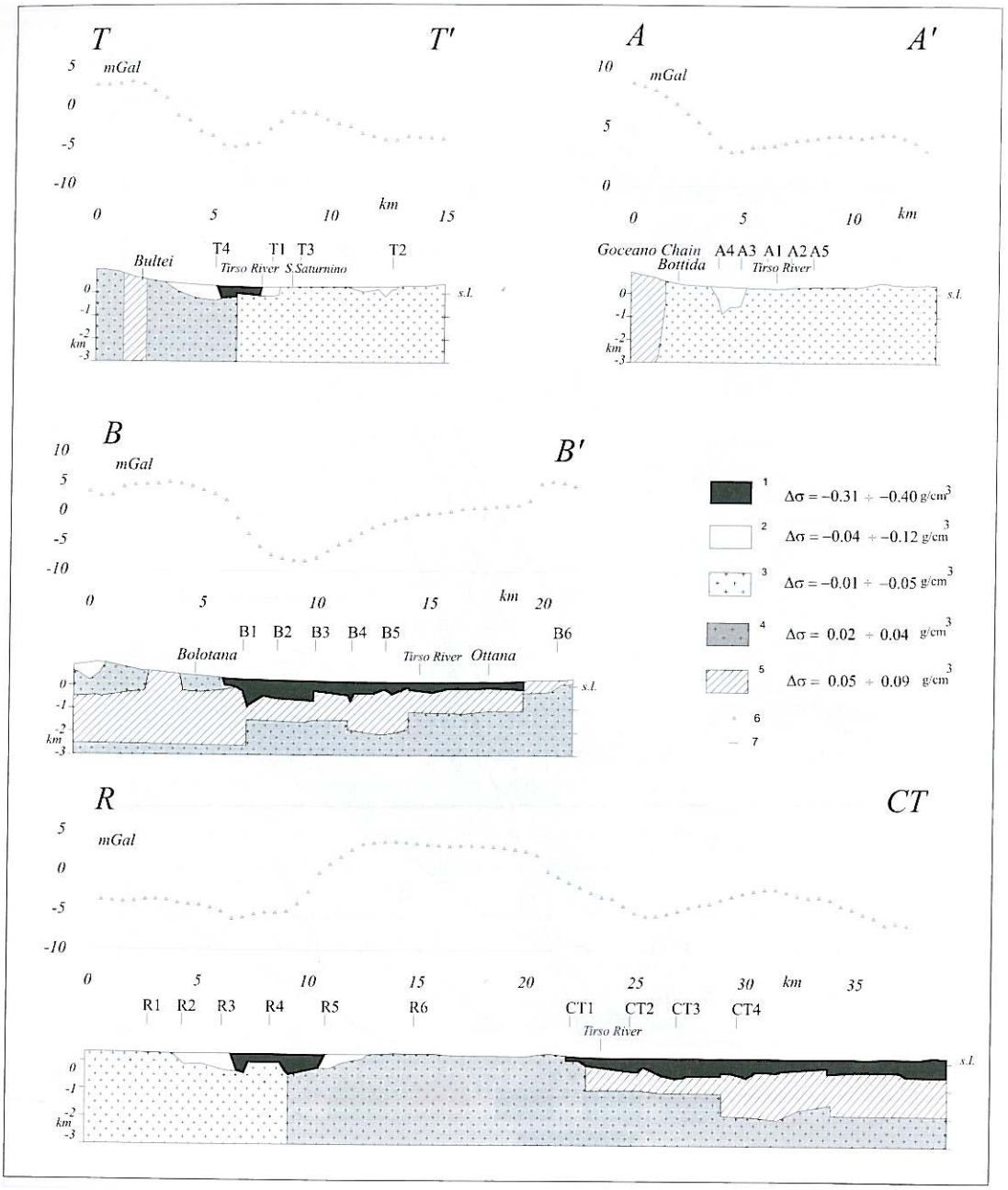

Fig. 9. Gravity models for T-T′, A-A′, B-B′ and R-CT profiles: 1) Tertiary-Quaternary volcano-sedimentary filling; 2) Oligo-Miocene ignimbritic-tuffaceous volcanic rocks; 3), 4) more or less weathered and fractured Paleozoic granitoids and schistose metamorphic rocks; 5) massive Paleozoic granitoids; 6) computed anomaly; 7) experimental anomaly.

ible modelling tool since it will interpret anomalies ranging from 2D to 3D, simply varying the ratio of the strike length with respect to the width length. Hence, it was profitably used in the present case, in spite of the lack of well defined symmetry of the gravity anomalies. The raw models were built using the subsurface geometry derived from interpretation of geoelectrical data. As for resistivity, available information on the outcropping rocks and density estimates obtained by means of field and laboratory measurements were considered. The latter were consistent with the density estimates used for neighbouring areas (Pecorini *et al.*, 1988; Balia *et al.*, 1990). Lastly, the association between density contrast relative to the regional background and rock type has been assumed as follows:

1) $-0.31 \div -0.40$ g/cm^3
   Tertiary-Quaternary volcano-sedimentary filling.

2) $-0.04 \div -0.12$ g/cm^3
   Oligo-Miocene ignimbritic-tuffaceous volcanic rocks.

3) $-0.01 \div -0.05$ g/cm^3
4) $0.02 \div 0.04$ g/cm^3
   More or less weathered and fractured Paleozoic granitoids and schistose metamorphic rocks.

5) $0.05 \div 0.09$ g/cm^3
   Massive Paleozoic granitoids.

As is known, the inversion procedure consists of iteratively varying the starting model parameters (shape, depth, density contrast, number of bodies) to minimize the RMS error between computed and experimental data. In the case at issue, the residual RMS error at the end of the iterative procedure was always less than 1% (namely 0.22% for T-T′; 0.13% for A-A′; 0.35% for B-B′; 0.23% for R-CT profiles).

Figure 9 shows the final gravity models; experimental and computed anomalies are reported in the upper part.

After inversion, the gravity and resistivity models (fig. 6) maintain good agreement as far as shallow structures are concerned and, in particular, the boundary between Tertiary-Quaternary volcano-sedimentary filling and Paleozoic rocks remains substantially unchanged. However, some minor discrepancies can be observed for deeper structures. As an example, the massive Paleozoic granitoids to which the highest density is associated, do not show the highest resistivity, as probably expected. Apart from the different spatial sampling rates adopted in gravity and electrical surveying, these discrepancies can be attributed to the different correlation of density and resistivity with respect to mineralogical, lithological and hydrogeological variations.

In section T-T′, the gravity model shows the Oligo-Miocene rocks overlaying the transition to the Eastern Paleozoic horst granites, which should be the source of the long-wavelength gravity decrease (Trudu, 1962).

In section A-A′, the steep gradient corresponds to the transition from dense metamorphic outcrops of the Goceano chain again to granites of the Eastern Paleozoic horst.

The model corresponding to section B-B′ shows the Oligo-Miocene volcano-sedimentary sequence covering the Paleozoic basement in the Bolotana-Ottana area.

The NE-SW striking section R-CT crosses all previously modelled structures and confirms the volcano-sedimentary filling near Bultei, the dense tectonic sill in the central part and the features of the Bolotana-Ottana area. Here the total thickness of Quaternary sediments and Tertiary volcanic products can be estimated in the order of 700-800 m, in good agreement with seismic reflection data (De Cillia *et al.*, 1992).

4. Discussion

The above interpretation of geophysical data in terms of main geological structures of the Middle Tirso Valley provides fairly satisfactory quantitative information on more or less already known geological models. Aside from this, the geophysical data, in conjunction with the geological and structural information, allow us to draw the following considerations on one of

the most significant anomalies, the Bolotana-Sedilo gravity low:

1) It corresponds to considerably thick Pliocene basalt flows (100-300 m), Miocene marine-fluvial-lacustrine sediments (over 400 m) and, on the basis of our interpretation, Oligo-Miocene volcanic rocks (at least 800-1000 m).

2) It is bounded by the Marghine fault and the Marghine chain northwards and probably by the Nuoro fault southwards, but the latter connection is not clearly supported by our geophysical data. Moreover, the eastern edge of the gravity low seems to be related to the NNE-SSW regional sequence of extensive tectonic structures which follows the line of the San Saturnino, Oddini and Fordongianus thermal springs. The sequence of these structures, which cannot always be easily recognized in the field being overlain by the Pliocene-Quaternary basaltic and alluvial cover, can be suitably named «Tirso Fault» for the first time.

3) If the Marghine fault is interpreted as the south-eastern prolongation of the transcurrent Tavolara fault (fig. 1), the features of the Bolotana-Sedilo gravity low are typical of a Tertiary volcano-sedimentary basin, bounded by two master faults: the transcurrent Tavolara-Marghine fault, and the normal-extensional Tirso fault along which geothermal phenomena occur.

Summing up, this is a tectonic depression with complex characteristics, including the calk-alcaline volcanism, typical of a pull apart basin which well matches the geodynamic rifting and rotational events that took place in Sardinia during the Oligocene-Lower Miocene.

Although the results of the present survey warrant further integration and validation, the considerations that can be drawn therefrom concerning the main structural features of the Middle Tirso Valley and their relationships with the Tertiary volcanism in Sardinia, should form a sound basis for future geological, volcanological and geodynamical research, as well as for more practical fields of interest such as groundwater and geothermal resources assessment.

REFERENCES

ALPIN, L.M. (1966): *Dipole Methods for Measuring Earth Conductivity* (Translation from Russian), Plenum Press, New York.

BALIA, R., M. CIMINALE, M. LODDO, D. PATELLA, G. PECORINI and A. TRAMACERE (1990): Geophysical study of the Fordongianus geothermal area (Sardinia Island, Italy), *Boll. Geofis. Teor. Appl.*, **22**, 129-140.

BECCALUVA, L., P. BROTZU, G. MACIOTTA, L. MORBIDELLI, G. SERRI and G. TRAVERSA (1987): Cainozoic tectono-magmatic evolution and inferred mantle source in the Sardo-Tyrrhenian area, in *The Lithosphere in Italy: Advances in Earth Science Research*, Accademia Nazionale dei Lincei, Roma, 229-248.

CARMIGNANI, L. (1996): *Geologic Map of Sardinia*, edited by the «Comitato Regionale per il Coordinamento della Cartografia Geologica e Geotematica della Sardegna (Servizio Geologico Nazionale and Regione Autonoma della Sardegna).

CHERCHI, A. and L. MONTADERT (1982): The Oligo-Miocene rift of Sardinia and the early history of the Western Mediterranean basins, *Nature*, **298**, 736-739.

COULON, C., J. DOSTAL and C. DUPUY (1978): Petrology and geochemistry of the ignimbrites and associated lava domes from NW Sardinia, *Contrib. Mineral. Petrol.*, **68**, 89-98.

DE CILLIA, C., S. FAIS, A. PORCU and R. TOCCO (1992): Geostructural features of the middle Tirso valley from seismic reflection data, *Boll. Geofis. Teor Appl.*, **34**, 273-286.

GHEZZO, C., G. GUASPARRI and G. SABATINI (1973): Lineamenti geopetrografici del cristallino sardo. Le plutoniti e la loro successione negli eventi intrusivi, *Mineral. Petrogr. Acta*, **18**, 205-274.

LACOSS, R.T. (1971): Data adaptive spectral analysis methods, *Geophysics*, **36**, 661-775.

LAFEHR, T.R. (1991): An exact solution for the gravity curvature (Bullard B) correction, *Geophysics* , **56**, 1179-1184.

LODDO, M. and D. PATELLA (1977): Spectral analysis of voltage measurements for the interpretation of dipole geoelectrical soundings in low resistivity geothermal areas, *Geothermics*, **6**, 227-236.

MARSON, I. and C. Morelli (1978): First order gravity net in Italy. Paper read at the *8th Meeting of the International Gravity Commission, Paris, 12-16 September 1978.*

MEJU, M.A. (1992): An effective ridge regression procedure for resistivity data inversion, *Comput. Geosci.*, **18** (2/3), 99-118.

MORELLI, C., C. GANTER, T. HONKASALO, P.K. MC CONNELL, I.G. TANNER, B. SZABO, U. UOTILA and C.T. WHALEN (1974): The International Gravity Standardization Net 1971 (IGSN71), *Spec. Publ. No. 4.*, Int. Ass. of Geodesy, IUGG, pp.194.

MORITZ, D. (1984): Geodetic reference system 1980, *Bull. Géodésique*, **58**, 388-398.

OGGIANO, G. (1994): Lineamenti stratigrafico-strutturali del basamento del Goceano (Sardegna centro-settentrionale), *Boll. Soc. Geol. It.*, **113**, 105-115.

OGGIANO, G., S. PASCI and A. FUNEDDA (1995): Il bacino transtensivo di Chilivani-Berchidda: un esempio di

struttura transtensiva. Possibili relazioni con la geodinamica cenozoica del Mediterraneo occidentale, *Boll. Soc. Geol. It.*, **114**, 465-475.

OKABE, M. (1979): Analytical expressions for gravity anomalies due to homogeneous polyhedral bodies and translations into magnetic anomalies, *Geophysics*, **44**, 730-741.

PALA, A., G. PECORINI, A. PORCU and S. SERRA (1982): Schema geologico-strutturale della Sardegna, in *Ricerche Geotermiche in Sardegna con Particolare Riferimento al Graben del Campidano*, Consiglio Nazionale delle Ricerche - PFE - RF10, 7-24.

PASCI, S. (1997): Tertiary transcurrent tectonics of North-Central Sardinia, *Bull. Soc. Geol. France*, **168**, 301-312.

PATELLA, D. and A. TRAMACERE (1986): Geoelectric axial dipole sounding curves for a class of two-dimensional earth structures, *Geophys. Prospect.*, **34**, 424-444.

PECORINI, G., R. BALIA, M. CIMINALE, M. LODDO, D. PATELLA and A. TRAMACERE (1988): Studio geofisico del Logudoro e delle aree circostanti, *Boll. Soc. Geol. It.*, **107**, 547-560.

PORCU, A. (1983): Geologia del graben di Ottana (Sardegna centrale), *Rend. Sem. Fac. Sci. Univ. Cagliari*, **53**, 151-169.

TRUDU, R. (1962): Rilevamento gravimetrico della Sardegna, *Boll. Geofis. Teor. Appl.*, **4**, 299-399.

WEBRING, M. (1985): SAKI-FORTRAN program for generalized linear inversion of gravity and magnetic profiles, *Open File Rep. 85-122*, U.S. Geol. Surv., pp. 29.

(received April 6, 2001;
accepted August 29, 2001)